

Rigorous lower bounds for the domains of definition of extended generating functions

Béla Erdélyi, Jens Hoefkens, and Martin Berz

*Department of Physics and Astronomy and National Superconducting Cyclotron
Laboratory, Michigan State University, East Lansing, MI 48824*

(Dated: April 29, 2025)

The recently developed theory of extended generating functions of symplectic maps are combined with methods to prove invertibility via high-order Taylor model methods to obtain rigorous lower bounds for the domains of definition of generating functions. The examples presented suggest that there are considerable differences in the size of the domains of definition of the various types of generating functions studied. Furthermore, the types of generating functions for which, in general, large domains of definitions can be guaranteed were identified. The resulting domain sizes of these generators are usually sufficiently large to be useful in practice, for example for the long-term simulations of accelerator and other Hamiltonian system dynamics.

I. INTRODUCTION

It is well known that coordinate transformations of Hamiltonian systems that keep the Hamiltonian structure intact are called canonical transformations, or, in more modern terminology, symplectic maps [1–3]. The time evolutions of Hamiltonian systems are also symplectic. Any symplectic map can be represented in terms of a single scalar function, called the generating function. Until recently, only the four conventional Goldstein-type generators were well known [2]. Following the introduction of extended generating functions, it has been shown that to each symplectic map, infinitely many generating function types can be constructed [4]. In certain applications, such as long term simulation of accelerators and other Hamiltonian systems, it is important to maintain symplecticity during tracking [4–6]. One available method to achieve this is the generating function based symplectic tracking [4, 7, 8].

In principle, any of the valid generators could be used for tracking of a given Hamiltonian system. Although it can be shown that for any globally defined symplectic map, global generators can always be found [9], in practice their construction is not straightforward. Indeed, as shown in [1, 4], the representation of symplectic maps through generators commonly available in practice are often only locally valid. Frequently, the purpose of the simulations is to estimate the region of space where stable particle orbits can be found, the so-called non-wandering set, or dynamic aperture in the beam dynamics terminology. Hence, a sizable phase space region must be covered by tracking, and if the generating function method is used, the generating function must be defined at least in that region. However, so far nothing has been known about the size of the domains of definition of generating functions. The necessity to study this interesting problem has been recognized in [4, 7, 8, 10].

The purpose of this paper is to show that, using sophisticated high-order Taylor model based methods [11, 12], it is possible to rigorously prove lower bounds on the size of the domains of definition of any type of generating function. The resulting domains often enclose the dynamic apertures of the examples studied.

The structuring of the paper is as follows: in Section II the extended generating function theory is reviewed, and in Section III a brief description of the verified numerical tools utilized for bounding the domains of definition is presented. Finally, the performance of the methods is illustrated by four examples in Section IV: two polynomial maps in two and four dimensions, respectively, the Fermi-Pasta-Ulam system [13], and a representative example taken from beam physics.

II. THE EXTENDED GENERATING FUNCTION THEORY

Following the exposition of [4], we regard every map as a column vector. Let

$$\alpha = \begin{pmatrix} \alpha_1 \\ \alpha_2 \end{pmatrix} \quad (1)$$

be a diffeomorphism of a subset of \mathbb{R}^{4n} onto its image. Notice that α_i , $i = 1, 2$, are the first $2n$ and second $2n$ components of α . This entails that $\alpha_i : U \subset \mathbb{R}^{4n} \rightarrow V_i \subset \mathbb{R}^{2n}$. Let

$$\text{Jac}(\alpha) = \begin{pmatrix} A & B \\ C & D \end{pmatrix} \quad (2)$$

be the $4n \times 4n$ Jacobian of α , split into $2n \times 2n$ blocks. Let

$$\tilde{J}_{4n} = \begin{pmatrix} J_{2n} & 0_{2n} \\ 0_{2n} & -J_{2n} \end{pmatrix}, \quad (3)$$

where

$$J_{2n} = \begin{pmatrix} 0_n & I_n \\ -I_n & 0_n \end{pmatrix} \quad (4)$$

with the unit matrix I_n of appropriate dimension. A map α is called conformal symplectic if

$$(\text{Jac}(\alpha))^T J_{4n} \text{Jac}(\alpha) = \mu \tilde{J}_{4n}, \quad (5)$$

where μ is a non-zero real constant [14]. Also, we denote by \mathcal{I} the identity map of appropriate dimension. A map \mathcal{M} is called symplectic if its Jacobian M satisfies the symplectic condition [15], that is

$$M^T J M = J. \quad (6)$$

Henceforth, we will consider symplectic maps that are origin preserving, i.e. maps around a fixed point. We call a map a gradient map if it has symmetric Jacobian N . It is well known that, at least over simply connected subsets, gradient maps can be written as the gradient of a function (hence the name) [1], that is

$$N = \text{Jac}(\nabla F)^T. \quad (7)$$

(∇F is regarded as a row vector [16].) The function F is called the potential of the map.

The best way to formulate the main result of the extended generating function theory is the following theorem [4]:

Theorem 1 (Existence of extended generating functions) *Let \mathcal{M} be a symplectic map. Then, for every point z there is a neighborhood of z such that \mathcal{M} can be represented by functions F via the relation*

$$(\nabla F)^T = \left(\alpha_1 \circ \begin{pmatrix} \mathcal{M} \\ \mathcal{I} \end{pmatrix} \right) \circ \left(\alpha_2 \circ \begin{pmatrix} \mathcal{M} \\ \mathcal{I} \end{pmatrix} \right)^{-1}, \quad (8)$$

where $\alpha = (\alpha_1, \alpha_2)^T$ is any conformal symplectic map such that

$$\det(C(\mathcal{M}(z), z) \cdot Mz + D(\mathcal{M}(z), z)) \neq 0. \quad (9)$$

Conversely, let F be a twice continuously differentiable function. Then, the map \mathcal{M} defined by

$$M = (NC - A)^{-1} (B - ND) \quad (10)$$

is symplectic. The matrices A, B, C, D, M , and N are defined above.

The function F is called the generating function of type α of \mathcal{M} , and denoted by $F_{\alpha, \mathcal{M}}$. Theorem 1 says that, once the generator type α is fixed, locally there is a one-to-one correspondence between symplectic maps and scalar functions, which are unique up to an additive constant. The constant can be normalized to zero without loss of generality. Due to the fact that there exist uncountably many maps of the form (5), to each symplectic map one can construct infinitely many generating function types.

We note that (8) cannot be simplified, due to the fact that the entries in the equations have different dimensions. For instance, α_i maps $\mathbb{R}^{4n} \rightarrow \mathbb{R}^{2n}$ and $(\mathcal{M} \mathcal{I})^T$ maps $\mathbb{R}^{2n} \rightarrow \mathbb{R}^{4n}$. For more details see [4].

Therefore, for a given \mathcal{M} , the domain of definition of the generator of type α is the domain of invertibility of

$$\left(\alpha_2 \circ \begin{pmatrix} \mathcal{M} \\ \mathcal{I} \end{pmatrix} \right), \quad (11)$$

according to (8). Thus, finding the domain of definition of a generator is equivalent to finding the domain of invertibility of (11). A large class of generator types, which are utilized in practice, is the generators associated with linear maps α . These can be organized into equivalence classes $[S]$, associated with

$$\alpha = \left(\begin{array}{cc} -JL^{-1} & J \\ \frac{1}{2}(I + JS)L^{-1} & \frac{1}{2}(I - JS) \end{array} \right), \quad (12)$$

and represented by arbitrary symmetric matrices S [4]. The matrix L stands for the linear part of \mathcal{M} .

In the next section we present the methods utilized to prove lower bounds of the domains of definition of a variety of generators, or equivalently symmetric matrices S , for several given \mathcal{M} s.

III. RIGOROUS NUMERICAL ANALYSIS WITH TAYLOR MODELS

The relative accuracy of floating point number representations on computers is limited, usually to around 16 significant digits. However, interval analysis takes this into account and allows the computation of guaranteed enclosures for computational results: the result of every interval computation consists of two numbers. Thus, if x_r is the analytical result of some computation C , and $R = [x_l, x_u]$ is the corresponding result of interval analysis, then $x_r \in R$. On the other hand, interval analysis can also be seen as a computerization of set theory: starting with $I = [x_l, x_u]$ and some computation C , the result $C(I) = [y_l, y_u]$ contains the result of the computation C applied to *every* number contained in I . Further details on interval analysis can be found in [17–19].

Recently, Taylor models have been developed [11] as a combination of the well known map approach [1] and interval analysis to obtain guaranteed enclosures of functional descriptions. Details on applications of these methods in beam physics are given in [20, 21]. Loosely speaking, a Taylor model is a set of maps that are, in some yet-to-be specified way, close to a reference polynomial. We consider a box $\mathbf{D} \subset \mathbb{R}^v$ containing x_0 and assume $P_n : \mathbf{D} \rightarrow \mathbb{R}^w$ to be a polynomial of order n , where n, v, w are all integers. If we then take an open non-empty set $R \subset \mathbb{R}^w$, we call the collection $(P_n, x_0, \mathbf{D}, R)$ a *Taylor model of order n with reference point x_0 over \mathbf{D}* .

We say that f is contained in a Taylor model $T = (P_n, x_0, \mathbf{D}, R)$ if $P_n(x) - f(x) \in R$ for all $x \in \mathbf{D}$ and the n -th order Taylor series of f around x_0 equals P_n .

Methods have been developed that allow mathematical operations on Taylor models that preserve the inclusion relationships. For example, for two given Taylor models, T_1 and T_2 , methods have been developed that compute Taylor models for the sum S , and the product P , of T_1 and T_2 , i.e.

$$\begin{aligned} f_1 \in T_1, f_2 \in T_2 &\Rightarrow (f_1 + f_2) \in S \\ f_1 \in T_1, f_2 \in T_2 &\Rightarrow (f_1 \cdot f_2) \in P. \end{aligned}$$

Similarly, the other elementary operations and intrinsic functions have been extended to Taylor models such that the fundamental inclusion properties of Taylor models are maintained. For the exponential function, this means that we have developed algorithms that compute a Taylor model T_E from a given Taylor model T such that

$$f \in T \Rightarrow \exp(f) \in T_E$$

Lastly, the antiderivation, which is essentially the integration operation, extends naturally to Taylor models. It allows us to compute a Taylor model T_I from a given Taylor model T such that T_I contains primitives for each function f contained in T . Since the antiderivation does not fundamentally differ from other intrinsic functions on the set of Taylor models, it is often used in fundamental Taylor model algorithms. An important application of the antiderivation will be presented in (15).

More information on arithmetic and intrinsic functions on Taylor models can be found in [11, 22, 23].

One major advantage of Taylor model methods over regular interval analysis is that the accuracy of the enclosures obtained by Taylor models scales with the $(n + 1)$ -st order of the domain size [24]. Thus, the Taylor model approach is of particular advantage in the combination of Taylor models with high-order map codes like COSY INFINITY [25] and gives small guaranteed enclosures even for complicated high-order maps in many variables.

A. Guaranteed Invertibility of Maps

The Inverse Function Theorem makes local statements about invertibility of maps at points x_0 . On the other hand, interval methods allow us to *test* whether a given map is invertible over a whole region: assuming that we have a criterion that has to be satisfied for *each point* in a region for the function to be invertible, we can use interval methods to test the whole region *at once*.

One such criterion is given below in Theorem 2. While it does not lend itself very well to pure interval arithmetic, since normal interval methods model the inherent structure of the matrix M rather inefficiently, it has been shown in [12] that the Taylor model approach can be used to make full use of the specific row-structure of M .

Theorem 2 (Invertibility from First Derivatives) *Let $\mathbf{B} \subset \mathbb{R}^v$ be a box and $f : \mathbf{B} \rightarrow \mathbb{R}^v$ a \mathcal{C}^1 function. Assume that the matrix*

$$M = \begin{pmatrix} \frac{\partial f_1}{\partial x_1}(\chi_1) & \cdots & \frac{\partial f_1}{\partial x_v}(\chi_1) \\ \vdots & & \vdots \\ \frac{\partial f_v}{\partial x_1}(\chi_v) & \cdots & \frac{\partial f_v}{\partial x_v}(\chi_v) \end{pmatrix} \quad (13)$$

is invertible for every choice of $\chi_1, \dots, \chi_v \in \mathbf{B}$. Then f has a \mathcal{C}^1 -inverse defined on the whole set $f(\mathbf{B})$, where $f(\mathbf{B})$ denotes the range of f over \mathbf{B} .

It has been shown in [12] that a Taylor model implementation of Theorem 2 can successfully determine invertibility of complicated high-dimensional functions over large regions \mathbf{B} . We do, however, point out that an application of this theorem cannot disprove invertibility of a given map.

B. Verified Enclosures of Flows

Another important application of Taylor models stems from their applicability to numerical ODE integration. To illustrate how this works, we consider the initial value problem

$$x' = f(t, x) \quad \text{and} \quad x(t_0) = x_0. \quad (14)$$

It is a well known fact that the solution to (14) can be obtained as the fixed point of the Picard operator \mathcal{O} , defined by

$$\mathcal{O}(x) = x_0 + \int_{t_0}^t f(\tau, x) d\tau. \quad (15)$$

Using the previously mentioned antiderivation, the operator \mathcal{O} can be extended to Taylor models and yields an algorithm that allows the computation of verified *enclosures of flows* of (14). This approach has been presented in [26, 27] and has recently been used successfully in a variety of applications ranging from solar system dynamics [28] to beam physics. Unlike methods that use regular interval computations to enclose the final conditions, the Taylor model approach avoids the wrapping effect to very high order. It is therefore capable of propagating extended initial regions over large integration intervals.

If we denote the solution of (14) by $\mathcal{M}(t, t_0, x_0)$, we consider the corresponding matrix initial value problem

$$Y' = \left(\frac{\partial f}{\partial x}(t, \mathcal{M}(t, t_0, x_0)) \right) \cdot Y, \quad Y(t_0) = I. \quad (16)$$

We use Taylor model methods to compute Taylor models containing the map $\mathcal{M}(t_f, t_0, x_0)$ at the final time t_f . Moreover, since $\frac{\partial \mathcal{M}}{\partial x_0}$ satisfies (16), we also obtain Taylor models containing the derivatives $\frac{\partial \mathcal{M}}{\partial x_0}(t_f, t_0, x_0)$ at that final point. The latter is required for a determination of invertibility of (11) based on Theorem 2.

IV. EXAMPLES

A. A cubic 2D symplectic map

As a first example we consider a two dimensional cubic polynomial, which is exactly symplectic. It has the following form:

$$\mathcal{M} = \mathcal{N} \circ \mathcal{L}, \quad (17)$$

where

$$\mathcal{L} = \begin{pmatrix} \cos \frac{\pi}{3} & \sin \frac{\pi}{3} \\ -\sin \frac{\pi}{3} & \cos \frac{\pi}{3} \end{pmatrix}, \quad (18)$$

and

$$\mathcal{N} \begin{pmatrix} q \\ p \end{pmatrix} = \begin{pmatrix} q - 3(q+p)^3 \\ p + 3(q+p)^3 \end{pmatrix}. \quad (19)$$

This simple example even lends itself to an analytical treatment. Applying Theorem 2, we obtain the following determinant in the four variables q_1, p_1, q_2, p_2 :

$$\begin{aligned} & 1 + 9 \frac{[(1 - \sqrt{3}) q_1 + (1 + \sqrt{3}) p_1]^2}{8 (1 + \sqrt{3})^2} \left[(2 + \sqrt{3}) (s_{12} + 1) + s_{22} \right] \\ & + 9 \frac{[(1 - \sqrt{3}) q_1 + (1 + \sqrt{3}) p_1]^2}{8 (1 + \sqrt{3})^2} \left[(2 + \sqrt{3}) (s_{12} - 1) + (7 + 4\sqrt{3}) s_{11} \right], \end{aligned} \quad (20)$$

where

$$S = \begin{pmatrix} s_{11} & s_{12} \\ s_{12} & s_{22} \end{pmatrix}. \quad (21)$$

Theorem 2 guaranties globally defined inverses if (20) is positive definite. Clearly, this is the case if

$$s_{22} \leq (2 + \sqrt{3})(s_{12} + 1) \quad (22)$$

$$s_{11} \leq \frac{2 + \sqrt{3}}{7 + 4\sqrt{3}}(s_{12} - 1), \quad (23)$$

for any s_{12} . Therefore, we are able to prove that there is a large class of generators that is globally defined for this symplectic map.

However, these solutions are not unique, and we are interested mainly in proving invertibility in finite regions that enclose the dynamic aperture. For these cases, the Taylor model based method described in Section III is well suited. For example, employing the Taylor method for the $S = 0$ case, the tracking picture shown in Fig. 1 was obtained. The box surrounding the tracking is the region for which invertibility of the corresponding generator can be proved. Clearly, it goes well beyond the dynamic aperture, which is approximately 0.2. To check invertibility for other generators, we created a few random generator types, based on random symmetric matrices with entries uniformly distributed in $[-10, 10]$. The results are presented in Table I.

B. A 4D symplectic map

The second example is somewhat more complex. While staying in the category of polynomial symplectic maps, the dimensions were doubled (4D), and to ensure exact symplecticity, we composed two types of maps that are known to be symplectic, namely rotations

$$\mathcal{R} = \begin{pmatrix} R_1 & 0 \\ 0 & R_2 \end{pmatrix}, \quad (24)$$

where

$$R_i = \begin{pmatrix} \cos \frac{\pi}{3} & \sin \frac{\pi}{3} \\ -\sin \frac{\pi}{3} & \cos \frac{\pi}{3} \end{pmatrix}, \quad (25)$$

$i = 1, 2$, and kicks

$$\mathcal{K}_i \begin{pmatrix} \vec{q} \\ \vec{p} \end{pmatrix} = \begin{pmatrix} \vec{q} \\ p_i + \frac{q_i}{\partial q_i} f(\vec{q}) \end{pmatrix}, \quad (26)$$

where $\vec{p} = (p_1, p_2)^T$, and f is any polynomial of $\vec{q} = (q_1, q_2)^T$.

For a typical example (with $f(q_1, q_2) = 1.5q_1q_2 + q_1^2 + 2(q_1 + q_2)^3 + 1.45(1.1q_1 - 0.5q_2)^4$), we obtained the tracking pictures depicted in Figs. 2 and 3. Fig. 2 shows some particles launched relatively close to the origin, where the system is still weakly nonlinear, and the behavior of the particles is similar to those in a real accelerator. However, the dynamic aperture is much bigger, and lies somewhere in the more nonlinear region, close to the particles tracked in Fig. 3. As in the previous example, in Fig. 3 the lower bounds for invertibility of the case $S = 0$ are also shown. In fact, long term tracking shows that the dynamic aperture is approximately 0.036 in q_1 and 0.052 in the q_2 directions. Applying the Taylor method to a variety of generators we found the lower bounds for the domains shown in Table II. Notice that several generators can be guaranteed to be defined beyond the dynamic aperture.

C. The Fermi-Pasta-Ulam system

The first two examples have been fabricated such that the corresponding symplectic maps are polynomial and known to arbitrary precision. This is not usually the case for problems encountered in practice. The information that is supposed to be known exactly are the Hamiltonian functions, or equivalently, the corresponding ordinary differential equations. Since closed form solutions are almost never available, the solutions are usually approximated, for example

by Taylor series. Using verified integration methods, we can enclose the true solution by a Taylor model. The Taylor model contains many symplectic (and non-symplectic) maps, one of which is the exact solution. Therefore, applying the invertibility tests to the Taylor model containing the true solution of the ODE, we can again prove lower bounds for domains of generating functions.

A famous Hamiltonian system is the Fermi-Pasta-Ulam system shown in Fig. 4 [13]. It is a paradigmatic model for nonlinear classical systems, which is known to exhibit many interesting features, and stimulated important developments in nonlinear dynamics. It is determined by the Hamiltonian

$$H(\vec{q}, \vec{p}) = \frac{1}{2} \sum_{i=1}^n (p_{2i-1}^2 + p_{2i}^2) + \frac{k}{2} \sum_{i=1}^n (q_{2i} - q_{2i-1})^2 + \sum_{i=0}^n (q_{2i+1} - q_{2i})^4. \quad (27)$$

For our specific example we took $n = 2$ ($q_4 = q_5 = p_4 = 0$), and $k = 5000$. Employing the Taylor model based verified integrator, we obtained the Taylor model of one half period map of the flow of (27), and then tracked some particles by iteration of the map. Typical phase space plots are presented in Fig. 5. The domain of the generator associated with $S = 0$ extends to at least $[-1, 1]$ in every direction in phase space. Since there is no real dynamic aperture in this case, to compare different generating function types a set of 1000 random symmetric matrices were created with entries in $[-1, 1]$. Then the corresponding generator types were constructed. Furthermore, the symmetric matrices were multiplied by constants between $[0, 1]$ to investigate the percentage of generators associated to these matrices that are still defined over $[-1, 1]$ in every direction in phase space. As shown in Fig. 6, there is a sharp increase in the fraction of generators defined over the whole region of interest as the “size” of the symmetric matrices decrease. If S is small enough, the generator type associated with it is defined over $[-1, 1]$.

D. An accelerator cell

We conclude the section with an example of practical interest in accelerator physics. The Hamiltonian representing an accelerator magnet, with the arclength s as independent variable, and on-energy particles is

$$H(x, y, a, b) = - \left(1 + \frac{x}{\rho} \right) \sqrt{1 - a^2 - b^2} - \frac{q}{p_0} \left(1 + \frac{x}{\rho} \right) A_s(x, y), \quad (28)$$

where ρ is the curvature radius of the magnet, A_s is the s component of the vector potential, and $((x, a); (y, b))$ are two pairs of canonically conjugate variables. For the sake of computational simplicity, we assume that the magnetic fields are piecewise independent of the arclength, in particular we use the sharp cutoff approximation for fringe fields, as is commonly done in beam physics. Specifically, for field free space $\rho = \infty$ and $A_s = 0$, for a homogeneous dipole magnet

$$A_s = -\frac{B_0}{2} (x + \rho), \quad (29)$$

where $qB_0/p_0 = 1/\rho$, for a quadrupole $\rho = \infty$ and

$$A_s = -\frac{k}{2} (x^2 - y^2), \quad (30)$$

where k is the quadrupole strength ($k > 0$ means focusing in the x direction, and $k < 0$ means defocusing in the x direction and focusing in the y direction), and for a sextupole $\rho = \infty$ and

$$A_s = -\frac{h}{3} (x^3 - xy^2), \quad (31)$$

where h is the sextupole strength. Combining these types of elements, we set up a cell, which consists of the following sequence of elements: drift, defocusing quadrupole superimposed with a sextupole, drift, bending dipole, drift, defocusing quadrupole superimposed with a sextupole, and drift (Fig. 7). The defocusing quadrupoles have the same strength $k = -0.0085$, and the sextupole strength is $h = 0.06$. The length of the drifts are 1 m , of the quadrupoles and the dipole 0.5 m , and the dipole’s curvature radius $\rho = 2.5\text{ m}$. Integration over this structure yielded a Taylor model containing the true solution. Moreover, the final Taylor model encloses the final conditions with a relative overestimation in the order of 10^{-10} . Thus, the Taylor model approach does not only give verified enclosures of the flow, but it also leads to only marginal overestimation in the process. This result underscores the previously mentioned avoidance of the wrapping effect by the Taylor model approach. As an example of this, consider the Taylor

model shown in Table III. By providing a rigorous remainder bound, it describes a guaranteed enclosure of the final x positions as a polynomial function of the initial conditions x_0 , a_0 , y_0 , and b_0 at the end of the accelerator cell. For increase readability, only terms of orders three or less have been listed (the actual computations were done in order 17 and the reference polynomial has a total of 1933 non-vanishing terms). Note that the initial regions are all scaled to $[-1, 1]$ internally (naturally, the polynomial coefficients have been scaled accordingly).

As for the Fermi-Pasta-Ulam system, a plot was created, which shows the percentage of a set of 1000 random generators defined over a phase space region of $[-0.1, 0.1]$ in every direction. The value of 0.1 approximately corresponds to a typical accelerator magnet aperture, and includes the dynamic aperture, which is estimated from tracking to be $(x, y) = (0.03, 0.045)$, as shown in Fig. 8. Clearly, the trend is the same as for the Fermi-Pasta-Ulam system: for smaller S there is a larger chance that the associated generating function is defined over the region of interest, and if S is close enough to zero, 100% of the generators are defined (Fig. 9).

Finally, we note that the size of the domains of definition of the extended generating functions is directly related to the problem of optimal symplectic approximation of Hamiltonian flows [9]. The conclusion reached in this paper are confirmed by a very general theoretical argumentation based on Hofer's metric; in general the generating function associated with $S = 0$ gives the optimal approximation. This suggests that the $S = 0$ generator, as shown in Figs. 6 and 9, is not the best because the Taylor model based tools utilized to prove lower bounds for the domains of definition happen to work best for small symmetric matrices S .

-
- [1] M. Berz, *Modern Map Methods in Particle Beam Physics* (Academic Press, San Diego, 1999).
 - [2] H. Goldstein, *Classical Mechanics* (Addison-Wesley, Reading, MA, 1980).
 - [3] J. M. Sanz-Serna and M. P. Calvo, *Numerical Hamiltonian Problems* (Chapman and Hall, London, 1994).
 - [4] B. Erdelyi and M. Berz, Theory of extended generating functions for symplectification of truncated Taylor maps, Phys. Rev. ST-Accel. Beams **submitted** (2000, preliminary version available at <http://130.83.124.174/frames/index.htm>).
 - [5] I. Gjaja, A. Dragt, and D. Abell, A comparison of methods for long-term tracking using symplectic maps, IOP Conf. Ser. **131**, 173 (1993).
 - [6] D. Abell, *Analytic properties and approximation of transfer maps for Hamiltonian systems*, Ph.D. thesis, University of Maryland (1995).
 - [7] M. Berz, Symplectic tracking in circular accelerators with high order maps, in *Nonlinear Problems in Future Particle Accelerators* (World Scientific, Singapore, 1991) p. 288.
 - [8] R. Warnock and J. Ellison, From symplectic integrator to Poincare map: spline expansion of a map generator in Cartesian coordinates, Appl. Numer. Math. **29**, 89 (1999).
 - [9] B. Erdelyi, *Optimal Approximation of Hamiltonian Flows and Accurate Simulation of Fringe Field Effects*, Ph.D. thesis, Michigan State University, East Lansing, MI, USA (2001).
 - [10] P. Channell, Hamiltonian suspensions of symplectomorphisms: an alternative approach to design problems, Physica D **127** (3-4), 117 (1999).
 - [11] K. Makino and M. Berz, Remainder differential algebras and their applications, in *Computational Differentiation: Techniques, Applications, and Tools*, edited by M. Berz, C. Bischof, G. Corliss, and A. Griewank (SIAM, Philadelphia, 1996) pp. 63–74.
 - [12] J. Hoeffkens and M. Berz, Verification of invertibility of complicated functions over large domains, Reliable Computing (in print, 2001, available at <http://bt.nsl.msu.edu/papers-cgi/display.pl?name=acainv00>).
 - [13] J. Ford, The Fermi-Pasta-Ulam problem: Paradox turns discovery, Phys. Rep. **213**, 271 (1992).
 - [14] A. Banyaga, *The structure of classical diffeomorphism groups* (Dordrecht, Boston, Kluwer Academic, 1997).
 - [15] A. J. Dragt, Lectures on nonlinear orbit dynamics, in *1981 Fermilab Summer School* (AIP Conference Proceedings Vol. 87, New York, 1982).
 - [16] R. Abraham, J. E. Marsden, and T. Ratiu, *Manifolds, Tensor Analysis, and Applications* (Springer-Verlag, New York, 1988).
 - [17] R. E. Moore, *Interval Analysis* (Prentice-Hall, Englewood Cliffs, New Jersey, 1966).
 - [18] E. Hansen, *Topics in Interval Analysis* (Oxford University Press, London, 1969).
 - [19] R. E. Moore, *Methods and Applications of Interval Analysis* (SIAM, Philadelphia, 1979).
 - [20] K. Makino, Rigorous integration of maps and long-term stability, in *1997 Particle Accelerator Conference* (APS, Vancouver, B.C., Canada, 1997).
 - [21] K. Makino and M. Berz, Verified integration of transfer maps, Physical Review ST-AB (submitted).
 - [22] K. Makino and M. Berz, Efficient control of the dependency problem based on Taylor model methods, Reliable Computing **5**, 3 (1999).
 - [23] M. Berz and G. Hoffstätter, Computation and application of Taylor polynomials with interval remainder bounds, Reliable Computing **4**, 83 (1998).
 - [24] M. Berz and J. Hoeffkens, Verified inversion of functional dependencies and superconvergent interval Newton methods, Reliable Computing **7** (2001).
 - [25] M. Berz, *COSY INFINITY Version 8 Reference Manual*, Tech. Rep. MSUCL-1088 (National Superconducting Cyclotron

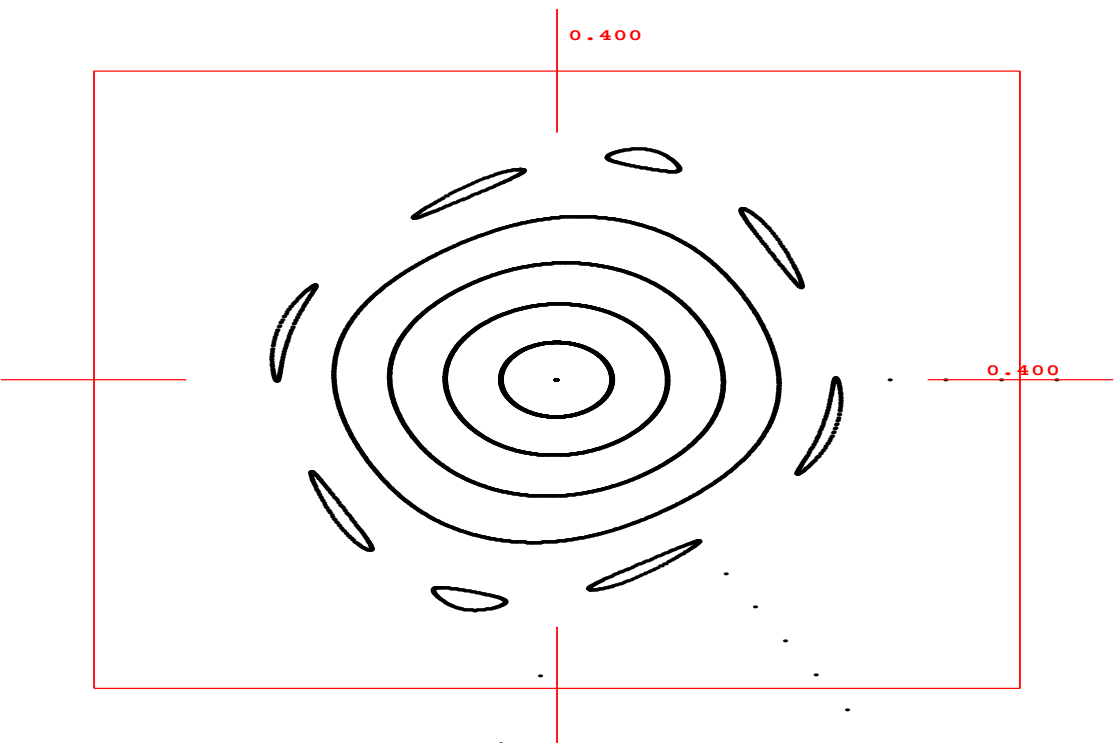


FIG. 1. Tracking picture of the cubic two dimensional symplectic map, and the box of guaranteed invertibility of the generator associated with $S = 0$.

- Laboratory, Michigan State University, East Lansing, MI 48824, 1997) see also <http://www.beamtheory.nsl.msu.edu/cosy>.
- [26] M. Berz and K. Makino, Verified integration of ODEs and flows with differential algebraic methods on Taylor models, *Reliable Computing* **4**, 361 (1998).
 - [27] K. Makino, *Rigorous Analysis of Nonlinear Motion in Particle Accelerators*, Ph.D. thesis, Michigan State University, East Lansing, Michigan, USA (1998), also MSUCL-1093.
 - [28] M. Berz, K. Makino, and J. Hoefkens, Verified integration of dynamics in the solar system, *Nonlinear Analysis* (in print).

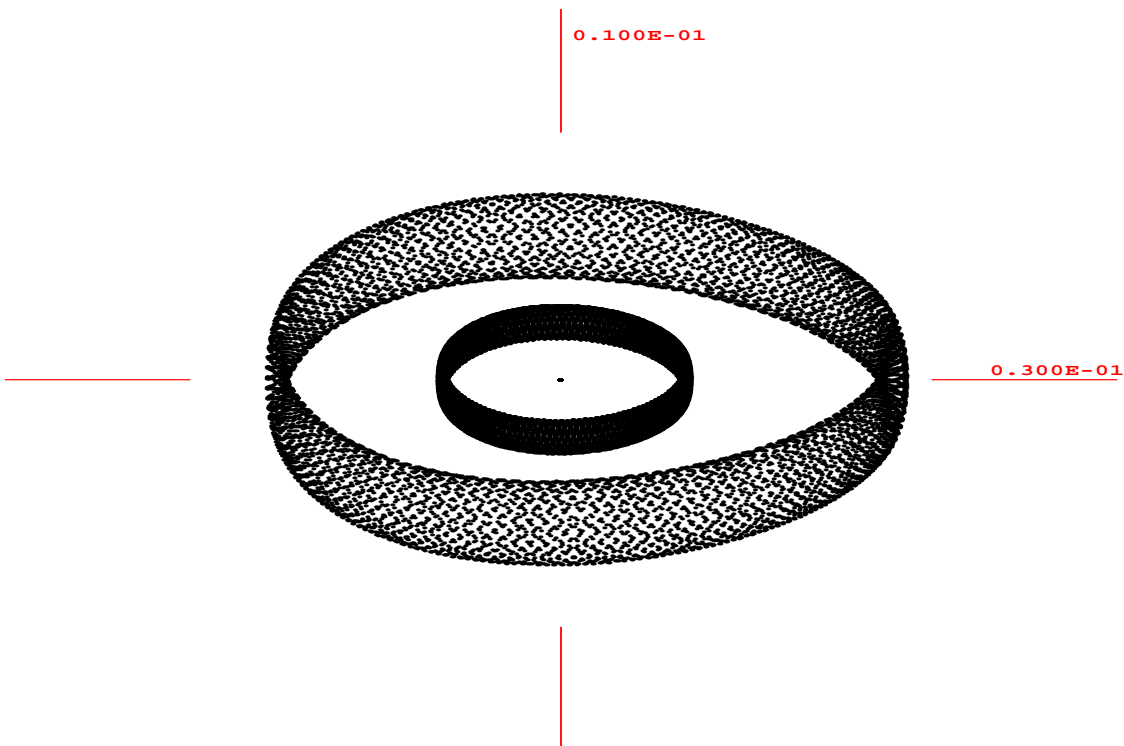


FIG. 2. (q_1, p_1) tracking picture of the four dimensional symplectic polynomial, for two initial conditions launched along the q_1 axis close to the origin.

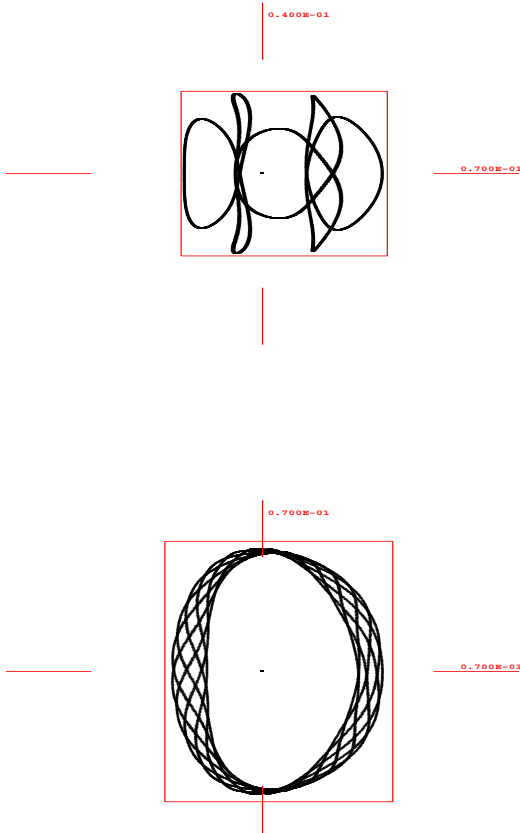


FIG. 3. (a) (q_1, p_1) , and (b) (q_2, p_2) tracking pictures of the four dimensional symplectic polynomial for two particles (launched along the q_1 and q_2 axes respectively) close to the dynamic aperture, and the box of guaranteed invertibility of the generator associated with $S = 0$.

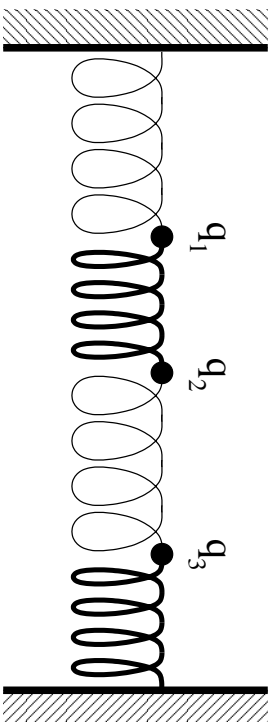


FIG. 4. The Fermi-Pasta-Ulam system used in our example.

TABLE I. Lower bounds for the domains of definition of several generating function types for the two dimensional cubic symplectic polynomial. The matrices S_1 through S_{10} are randomly generated with entries in $[-10, 10]$.

$[S]$ $(q_1; p_1)$ lower bounds for the domain of the generator	
0	$([-0.333, 0.333]; [-0.333, 0.333])$
I	$([-0.310, 0.310]; [-0.310, 0.310])$
S_1	$([-0.301, 0.301]; [-0.301, 0.301])$
S_2	$([-0.261, 0.261]; [-0.261, 0.261])$
S_3	$([-0.258, 0.258]; [-0.258, 0.258])$
S_4	$([-0.360, 0.360]; [-0.360, 0.360])$
S_5	$([-0.377, 0.377]; [-0.377, 0.377])$
S_6	$([-0.109, 0.109]; [-0.109, 0.109])$
S_7	$([-0.111, 0.111]; [-0.111, 0.111])$
S_8	$([-0.105, 0.105]; [-0.105, 0.105])$
S_9	$([-0.090, 0.090]; [-0.090, 0.090])$
S_{10}	$([-0.042, 0.042]; [-0.042, 0.042])$

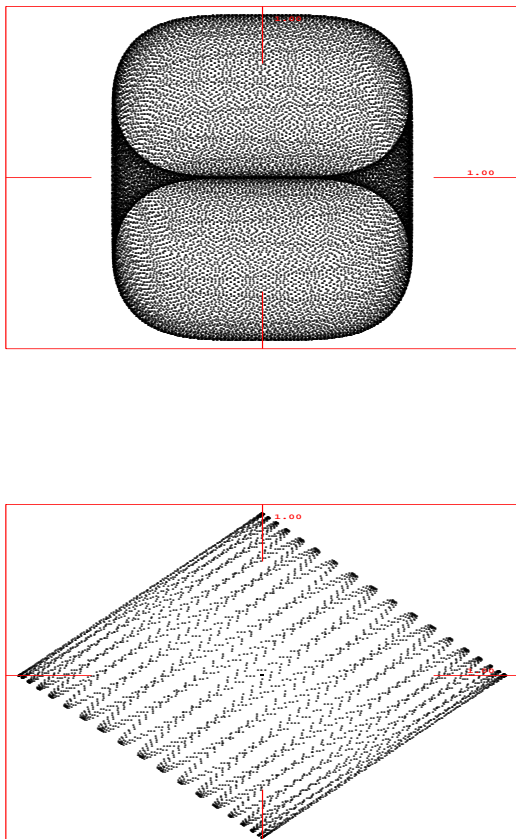


FIG. 5. (a) (q_1, p_1) , and (b) (q_1, q_2) tracking pictures of the half period map of the Fermi-Pasta-Ulam system for a particle launched along the q_1 axis. The box of guaranteed invertibility of the generator associated with $S = 0$ extends to at least $[-1, 1]$ in every direction.

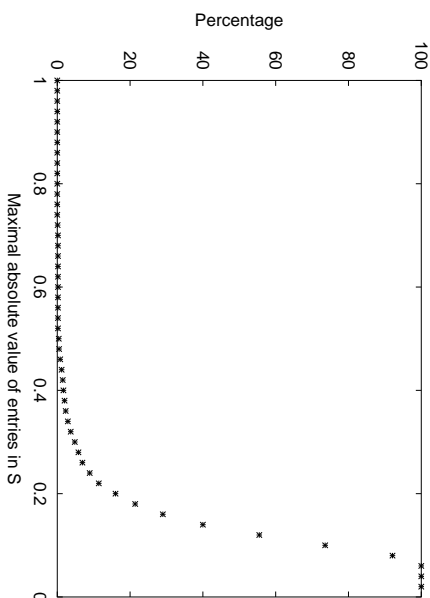


FIG. 6. The size of the random symmetric matrices S vs. the percentage of associated generators, which are defined at least up to $[-1, 1]$ in every direction in phase space for the Fermi-Pasta-Ulam system.

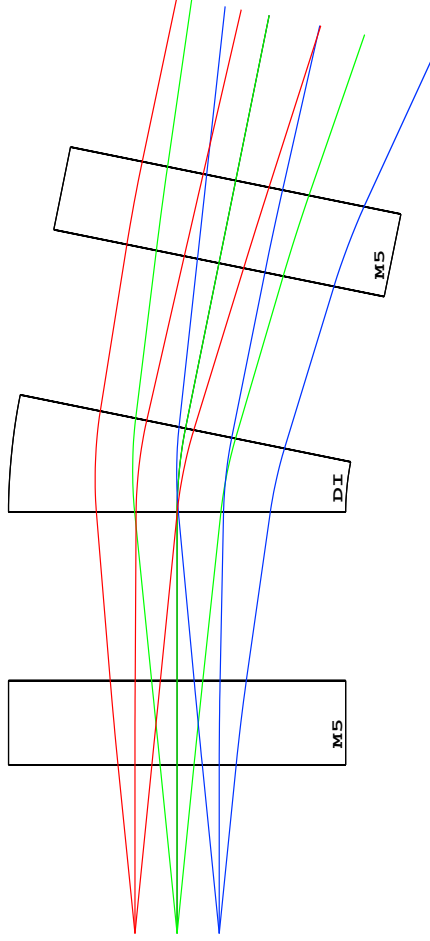


FIG. 7. The accelerator cell used in the example of Subsection IV D. The drifts are $1m$ long, the quadrupoles and the dipole are $0.5m$ long, and the dipole's radius of curvature is $2.5m$. The first quadrupoles are defocusing in the x direction, with strength $k = -0.0085$, and the reference particle is a $1MeV$ proton.

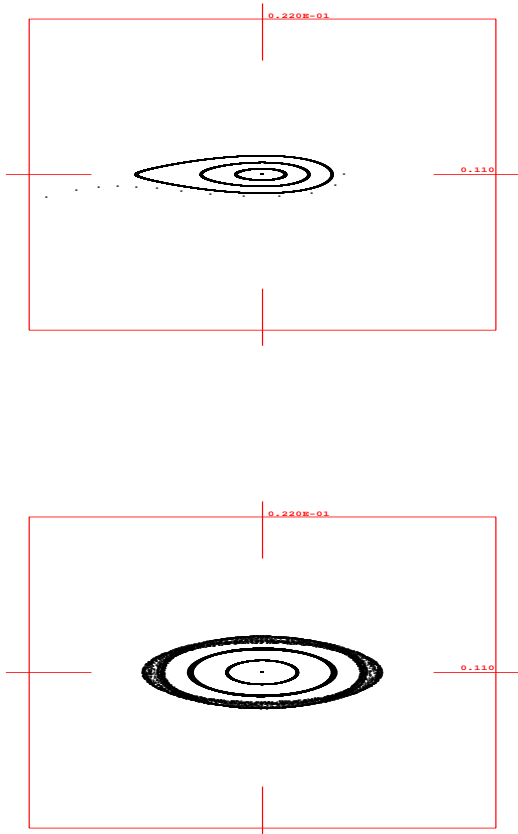


FIG. 8. (a) (x, a) , and (b) (y, b) tracking pictures of the one-turn map of the accelerator cell for particles launched along the x and y axes respectively. The box of guaranteed invertibility of the generator associated with $S = 0$ extends to at least $[-0.1, 0.1]$ in every direction.

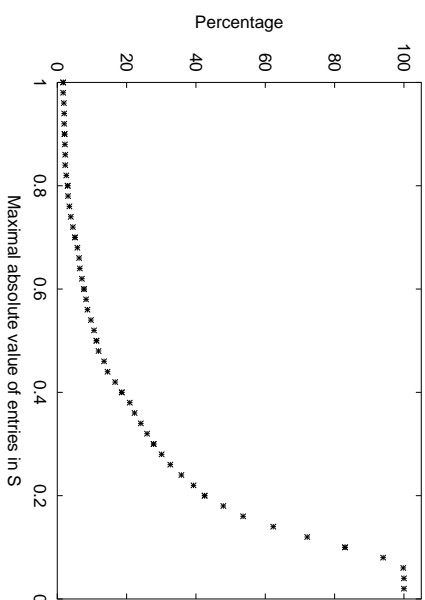


FIG. 9. The size of the random symmetric matrices S vs. the percentage of associated generators, which are defined at least up to $[-0.1, 0.1]$ in every direction in phase space for the accelerator cell.

TABLE II. Lower bounds for the domains of definition of several generating function types for the four dimensional symplectic polynomial. The matrices S_1 through S_{10} are randomly generated with entries in $[-10, 10]$.

$[S]$	$(q_1; p_1; q_2; p_2)$ lower bounds for the domain of the generator
0	$([-0.02220, 0.03404]; [-0.01924, 0.01924]; [-0.02664, 0.03552]; [-0.05328, 0.05328])$
I	$([-0.03742, 0.05738]; [-0.03243, 0.03243]; [-0.04491, 0.05988]; [-0.08982, 0.08982])$
S_1	$([-0.01732, 0.02656]; [-0.01501, 0.01501]; [-0.02079, 0.02772]; [-0.04158, 0.04158])$
S_2	$([-0.01610, 0.02474]; [-0.01398, 0.01398]; [-0.01936, 0.02582]; [-0.03873, 0.03873])$
S_3	$([-0.02112, 0.03238]; [-0.01830, 0.01830]; [-0.02534, 0.03379]; [-0.05068, 0.05068])$
S_4	$([-0.04900, 0.07514]; [-0.04247, 0.04247]; [-0.05880, 0.07840]; [-0.11761, 0.11761])$
S_5	$([-0.00967, 0.01483]; [-0.00838, 0.00838]; [-0.01161, 0.01548]; [-0.02322, 0.02322])$
S_6	$([-0.01630, 0.02500]; [-0.01413, 0.01413]; [-0.01956, 0.02608]; [-0.03913, 0.03913])$
S_7	$([-0.01489, 0.02283]; [-0.01290, 0.01290]; [-0.01787, 0.02383]; [-0.03574, 0.03574])$
S_8	$([-0.01186, 0.01819]; [-0.01028, 0.01028]; [-0.01423, 0.01898]; [-0.02847, 0.02847])$
S_9	$([-0.02064, 0.03164]; [-0.01788, 0.01788]; [-0.02476, 0.03302]; [-0.04953, 0.04953])$
S_{10}	$([-0.06874, 0.10540]; [-0.05957, 0.05957]; [-0.08249, 0.10999]; [-0.16498, 0.16498])$

TABLE III. Taylor model describing final x positions as a function of the initial conditions x_0, a_0, y_0, b_0 for the accelerator cell of subsection IV D.

RDA VARIABLE: NO= 17, NV= 4				
I	COEFFICIENT	ORDER	EXPONENTS	
1	0.1398389113940111	1	1	0 0 0
2	0.1038317686361456	1	0	1 0 0
3	-.2447944264979660E-01	2	2	0 0 0
4	-.1183394850192213E-01	2	1	1 0 0
5	-.2119694344941219E-02	2	0	2 0 0
6	0.2361409770673162E-01	2	0	0 2 0
7	0.1212766097410308E-01	2	0	0 1 1
8	0.2185093364668458E-02	2	0	0 0 2
9	0.9944830763540945E-03	3	3	0 0 0
10	0.8715481705011164E-03	3	2	1 0 0
11	0.1933878768639235E-03	3	1	2 0 0
12	0.3115908412345901E-04	3	0	3 0 0
13	0.1238155786756443E-02	3	1	0 2 0
14	-.1757616408645450E-03	3	0	1 2 0
15	0.1233139677764291E-02	3	1	0 1 1
16	0.8414517599464383E-04	3	0	1 1 1
17	0.1954684434876060E-03	3	1	0 0 2
18	0.4920452675843482E-04	3	0	1 0 2

VAR	REFERENCE POINT	DOMAIN INTERVAL		
1	0.0000000000000000	[-1.00000000 , 1.00000000]		
2	0.0000000000000000	[-1.00000000 , 1.00000000]		
3	0.0000000000000000	[-1.00000000 , 1.00000000]		
4	0.0000000000000000	[-1.00000000 , 1.00000000]		
ORDER	BOUND INTERVAL			
1	[-.2436706800301567 , 0.2436706800301567]			
2	[-.5056074647076302E-001, 0.4976080054742529E-001]			
3	[-.5066453459468558E-002, 0.5066453459468558E-002]			
R	[-.2157121190249145E-012, 0.2178948979195422E-012]			
